

# Large Strain Viscoelastic Model for Balloon Film

Kawai Kwok\* and Sergio Pellegrino†

*California Institute of Technology, Pasadena, CA 91125*

**This paper presents a constitutive model capable of predicting the anisotropic viscoelastic behavior of balloon film subject to large strains and cyclic loading. The model is based on the free volume theory of nonlinear viscoelasticity enhanced with a switching rule for treating loading and unloading differently. The model has been implemented in the finite element analysis program Abaqus/Standard and the results have been compared with experiments on the balloon film StratoFilm 420 under biaxial tension and shear.**

## I. Introduction

The NASA Superpressure Balloon program is developing stratospheric balloons to support scientific observations above 99% of the Earth's atmosphere with heavy payloads.<sup>1</sup> The current superpressure balloon design consists of a thin envelope made of linear low density polyethylene (LLDPE) film, contained within equally spaced meridional tendons.<sup>2</sup> A limiting factor in the design of these balloons is the existence of high stress concentrations in relatively small regions of the balloon film, for example near the edge of the cap region.

To enable the estimation of realistic factors of safety the actual stress concentrations in these regions need to be predicted, which requires the availability of a large strain material model. StratoFilm 420, the LLDPE based film currently used for NASA superpressure balloons, is both viscoelastic and anisotropic.<sup>3</sup> A constitutive model that accurately predicts the anisotropic, viscoelastic material response at large strains will avoid over-conservative designs based on incorrect estimates of localized stress concentrations.

The present study formulates a viscoelastic model that captures the behavior of the film up to the point where the instantaneous stiffness of the material vanishes and non-recoverable deformation begins. The constitutive model is implemented in a finite element program and validated against experiments.

The paper begins with a literature review on nonlinear viscoelasticity theory. Section III formulates a large strain viscoelastic model for StratoFilm 420 based on the concept of free volume; this model is then implemented in Abaqus/Standard through a user-defined material subroutine. Section V compares the numerical results with a set of experiments and Section VI concludes the paper.

## II. Background

The Boltzmann superposition principle used in linear viscoelasticity is not directly applicable to nonlinear viscoelastic materials. Constitutive models based on the multiple integral approach were proposed but found limited usage due to the complexity of the resulting formulation and substantial laboratory characterization required. The first widely used nonlinear viscoelastic model is due to Schapery, who introduced a single integral formulation where nonlinearities appear in the constitutive equations as stress or strain dependent material parameters.<sup>4-6</sup>

A biaxial model for StratoFilm 420 based on the Schapery model was formulated by Rand and Sterling<sup>3</sup> and implemented in a finite element simulation to study the overall stress distribution in a superpressure balloon.<sup>7</sup> Recently, applicability limits of the Schapery model were established by comparing the predictions from the model to biaxial tensile strength tests.<sup>8</sup> Results from this study showed that the biaxial Schapery

---

\*Ph.D. Candidate in Aeronautics, Graduate Aerospace Laboratories, 1200 E. California Blvd. MC 205-45. [kwk5@caltech.edu](mailto:kwk5@caltech.edu)

†Joyce and Kent Kresa Professor of Aeronautics and Professor of Civil Engineering, Graduate Aerospace Laboratories, 1200 E. California Blvd. MC 301-46. AIAA Fellow. [sergiop@caltech.edu](mailto:sergiop@caltech.edu)

model can only capture the film behavior under moderate strain levels, and far away from the onset of permanent deformation.

Another single integral model is the free volume model presented by Knauss and Emri.<sup>9,10</sup> Instead of relying on stress or strain dependent material parameters that have no direct physical interpretation, Knauss and Emri postulated a relation between macroscopic deformation and time shift factor through the concept of free volume. Free volume is the intermolecular space in a polymer that allows for the motion of molecular chain motions in response to an imposed deformation, thus giving rise to the observed viscoelastic response. Chain mobility is enhanced when the free volume is increased, allowing for faster accommodation of the chains to the imposed deformation. Hence the free volume implicitly controls the time scale of the material. In the free volume model, macroscopic volume changes associated with thermal expansion, moisture swelling, and mechanical dilatation are correlated with the free volume and eventually influence the time shift factor.

The free volume model was extended to allow for finite-strain kinematics for predicting rubbery behavior of polymers by O'Dowd and Knauss<sup>11</sup> and modified to include distortional effects by Popelar and Liechti.<sup>12</sup> This modified version was implemented in finite element simulations to study nonlinear shear behavior,<sup>13</sup> but all these studies are limited to isotropic materials.

Both the Schapery model and the free volume model were found to be inadequate in predicting the unloading behavior in uniaxial cyclic tests.<sup>14</sup> In particular, the experimentally determined unloading path has a concave curvature while the models predict a convex path. The same discrepancy was observed for other nonlinear viscoelastic models,<sup>15</sup> including the distortion-modified free volume model.<sup>16</sup> Models with an incorrect unloading path curvature tend to underestimate the strain recovery during unloading. Among the attempts to remedy this problem, the unloading switch rule proposed by Xia et al. has demonstrated the ability to correct the curvature sign when incorporated into nonlinear viscoelastic models.<sup>14</sup>

### III. Viscoelastic Model Formulation

The particular balloon film under study is StratoFilm 420. This film is produced by a coextrusion process of three layers, resulting in directional dependent material properties.<sup>8</sup> In the current work, the film is modeled as an anisotropic membrane under plane stress conditions based on free volume theory. We first review the fundamentals of free volume viscoelasticity, and apply this theory to StratoFilm 420.

#### A. Review of Free Volume Theory

While a more detailed account of the free volume model is given by Knauss and Emri,<sup>9,10</sup> here we shall outline the key ideas that serve as the foundation for modeling a membrane under plane stress. The free volume model originates from linear viscoelasticity, where behavior over a finite range of time scales is often adequately modeled by a Prony series. The Prony series representation of uniaxial creep compliance is written as

$$D(t) = D_0 + \sum_{j=1}^n D_j (1 - e^{-(t/\rho_j)}), \quad (1)$$

where  $t$  is time,  $D_0$  is the instantaneous compliance,  $D_j$  are the Prony coefficients, and  $\rho_j$  are the retardation times.

In linear viscoelasticity the effects of temperature on the material behavior can be treated in the same manner through the time-temperature superposition principle,<sup>17</sup> which states that the compliance at temperature  $T$  and time  $t$  is the same as the compliance at a reference temperature  $T_0$  at a reduced time  $t'$ ,

$$D(t, T) = D(t', T_0), \quad t' = \frac{t}{a(T)}, \quad (2)$$

where  $a(T)$  is the time shift factor. One can relate the viscoelastic behavior at one temperature to that at another temperature by a shift in the time scale. For constant temperatures above the reference temperature, the time shift factor is less than unity and hence viscoelastic processes are accelerated relative to the reference temperature. When temperature varies with time, the reduced time is obtained by integration,

$$t'(t) = \int_0^t \frac{d\tau}{a(T(\tau))}. \quad (3)$$

The viscoelastic constitutive relation in terms of reduced time is given as

$$\epsilon(t) = \int_0^t D(t' - \tau') \dot{\sigma}(\tau) d\tau, \quad (4)$$

where  $\epsilon$  is strain and  $\sigma$  is stress.

In the free volume model, the constitutive equations, Eqs. (3) and (4), remain the same, but the time shift factor is no longer dependent only on the temperature  $T$ . It depends also on the volumetric strain  $\epsilon_v$ ,

$$a = a(T, \epsilon_v). \quad (5)$$

The time shift factor is expressed in terms of the free volume by

$$\log a = \frac{B}{2.303} \left( \frac{1}{f} - \frac{1}{f_0} \right), \quad (6)$$

where  $B$  is a material function,  $f$  denotes the fractional free volume and  $f_0$  is the fractional volume at some reference conditions. It is assumed that  $f$  is linearly related to the temperature change and the volumetric strain, by

$$f = f_0 + \alpha_v(T - T_0) + \epsilon_v, \quad (7)$$

where  $\alpha_v$  is the volumetric coefficient of thermal expansion. Combining Eq. (6) and Eq. (7) gives

$$\log a = \frac{-B}{2.303 f_0} \left[ \frac{\alpha_v(T - T_0) + \epsilon_v}{f_0 + \alpha_v(T - T_0) + \epsilon_v} \right]. \quad (8)$$

It can be shown that Eq. (8) reduces to the Williams-Landel-Ferry (WLF) equation in linear viscoelasticity in the case of negligible volumetric strain. In summary, the free volume model describes nonlinear viscoelastic response by means of Eqs. (1), (3), (4) and (8).

## B. Anisotropic Plane Stress Model

The free volume model is adopted for the balloon film and plane stress conditions are assumed. Finite strains and rotations are present during large deformations, making different stress and strain measures possible for constitutive modeling.<sup>18</sup> To satisfy the principle of objectivity, the model formulated herein is formulated in terms of the second Piola-Kirchoff stress  $P$  and the Green-Lagrange strain  $E$ , which form a conjugate pair. They are defined as

$$[P] = J[F^{-1}][\sigma][F^{-T}], \quad (9)$$

$$[E] = [F^T][F] - [I], \quad (10)$$

where  $[F]$  is the deformation gradient,  $[\sigma]$  is the Cauchy stress, and  $J$  is the Jacobian defined by  $J = \det[F]$ . The constitutive relation is given as

$$[E(t)] = \int_0^t [D(t' - \tau')] [\dot{P}(\tau)] d\tau, \quad (11)$$

where  $t'$  is the reduced time defined by Eqs. (3) and (8). The creep compliance  $D(t)$  takes the form

$$D(t) = \begin{bmatrix} D_{11}(t) & D_{12}(t) & D_{13}(t) & 0 \\ D_{12}(t) & D_{22}(t) & D_{23}(t) & 0 \\ D_{13}(t) & D_{23}(t) & D_{33}(t) & 0 \\ 0 & 0 & 0 & D_{66}(t) \end{bmatrix}, \quad (12)$$

where the 1-axis and 2-axis denote the machine and transverse direction of the film respectively, and the 3-axis is normal to the film. Under plane stress conditions the compliance is often written as a 3 by 3 matrix,

however the compliance matrix in Eq. (12) has the additional terms  $D_{13}$ ,  $D_{23}$  and  $D_{33}$  corresponding to the film behavior in the thickness direction. These coefficients are needed to compute the volumetric strain as an internal state variable in the free volume model.

Each entry in  $D(t)$  is represented by a Prony series in the form of Eq. (1). Although there are 7 independent compliance functions, only 6 are needed because  $D_{33}(t)$  is multiplied by zero in the case of plane stress. The material parameters  $B$ ,  $\alpha_v$ , and  $f_0$ , together with the compliance functions, provide a complete description of the material for implementing the free volume model.

### C. Material Parameters for StratoFilm 420

The viscoelastic properties of StratoFilm 420 have been characterized by Rand<sup>19,20</sup> who also derived the parameters for the Schapery model. Here we derive the corresponding parameters for the free volume model from Rand's data making certain assumptions on the film behavior in the thickness direction. These assumptions will be explicitly stated. Some of the required parameters have been obtained by carrying out additional material characterization tests.

The volumetric coefficient of thermal expansion is written as the sum of the linear coefficients of thermal expansion,

$$\alpha_v = \alpha_1 + \alpha_2 + \alpha_3, \quad (13)$$

where the subscript denotes the material direction. Both  $\alpha_1$  and  $\alpha_2$  were obtained as polynomial functions of temperature.<sup>21</sup> In this work we assume  $\alpha_3$  to be their average and the resulting  $\alpha_v$  is plotted in Fig. (1).

The material functions  $B$  and  $f_0$  are determined from Rand's time shift data, which were given in the form,<sup>19</sup>

$$\log a = \begin{cases} (T - 293.16)[7.33 \times 10^{-4}(T - 273.16) - 0.179133] & \text{if } T \geq 233.16 \text{ K;} \\ 3.1068 - 0.2350275(T - 273.16) & \text{if } T < 233.16 \text{ K.} \end{cases} \quad (14)$$

Since the time shift factor in Eq. (14) was obtained from creep tests at small strains, it is a close approximation to Eq. (8) with  $\epsilon_v = 0$  and  $T_0 = 293.16 \text{ K}$ ,

$$\log a = \frac{-B}{2.303f_0} \left[ \frac{\alpha_v(T - 293.16)}{f_0 + \alpha_v(T - 293.16)} \right]. \quad (15)$$

A nonlinear optimization procedure was performed to find  $B$  and  $f_0$  by minimizing the least square errors between Eqs. (14) and (15) subject to the constraints

$$\frac{B}{2.303f_0} = c_1, \quad (16)$$

$$\frac{f_0}{\alpha_v} = c_2. \quad (17)$$

where  $c_1$  and  $c_2$  are constants. The constraints are imposed so that the time shift factor is in accordance with the WLF equation for the case of infinitesimal deformation. The results from the least square procedure are plotted in Figs. (2) and (3).

The creep compliance of the film in the machine direction,  $D_{11}$ , is expressed as a Prony series of 15 terms at the reference temperature  $T_0 = 293.16 \text{ K}$ . The master curve is plotted in Fig. (4) and the corresponding Prony series terms are summarized in Table (1). The remaining in-plane compliances are assumed to be expressed by the same Prony series as the compliance in the machine direction, but multiplied by experimentally determined constants,<sup>3</sup> as follows

$$D_{12}(t) = -0.58D_{11}(t), \quad (18)$$

$$D_{22}(t) = (1.122 + 6.5895 \times 10^{-4}T - 6.609 \times 10^{-6}T^2)D_{11}(t), \quad (19)$$

$$D_{66}(t) = 4.45D_{11}(t). \quad (20)$$

The compliance functions  $D_{13}$  and  $D_{23}$  of StratoFilm 420 were not characterized by Rand. Because of the small thickness of the film, direct measurements of these properties would pose significant challenges. In

the present study,  $D_{13}$  and  $D_{23}$  were determined by fitting the model predictions to the results of uniaxial tensile tests.

Uniaxial tension tests on 38  $\mu\text{m}$  thick strips of StratoFilm 420 were conducted with an Instron materials testing machine equipped with a thermal chamber. Reflective targets were adhered to the specimen for strain measurements using laser extensometers. A type-T thermocouple was used to monitor the temperature throughout the tests. Prior to testing, the thermal chamber was maintained at  $T = 0^\circ$  for 1 hour to achieve stable thermal equilibrium. Specimens with machine and transverse direction oriented along the loading direction were stretched at a nominal strain rate of 0.1%/s to provide data for fitting  $D_{13}$  and  $D_{13}$  respectively.

The Prony series for  $D_{13}$  and  $D_{23}$  were assumed to have the same retardation times  $\rho_j$  as that of  $D_{11}$ , hence only the Prony coefficients were determined from the nonlinear least square fitting procedure. The results of these uniaxial tension tests and the corresponding numerical fits are shown in Fig. (5). The Prony series for  $D_{13}$  and  $D_{23}$  are plotted in Fig. (6), while the Prony coefficients are summarized in Table (2).

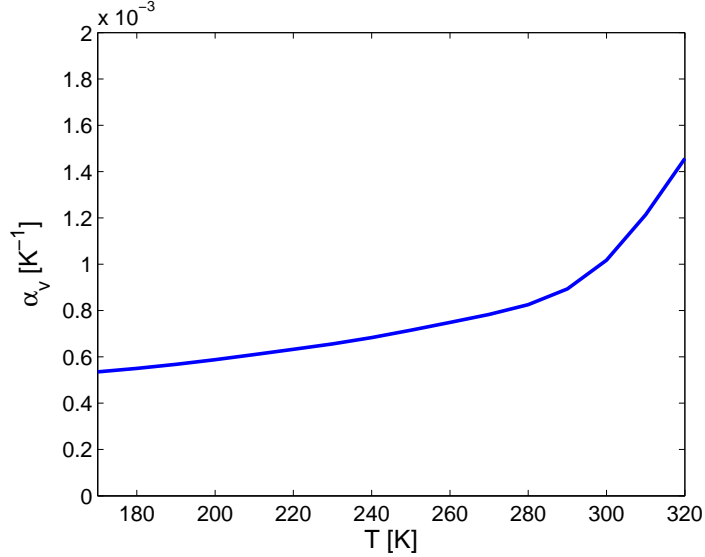


Figure 1: Volumetric coefficient of thermal expansion.

#### D. Unloading Behavior

To correctly simulate the unloading behavior, the switch rule proposed by Xia et al.<sup>14</sup> was modified and incorporated into the current free volume model. Xia et al. first distinguished between loading and unloading using a criterion based on the von Mises stress level experienced by the material. The criterion is checked throughout the deformation history. No correction is made when loading but when unloading is detected the nonlinear parameters in the viscoelastic model retain their values at the point of switching from loading to unloading. In the present free volume model, the criterion is based upon  $\epsilon_v$ . A local maximum in the volumetric strain history corresponds to switching from loading to unloading:

$$\left. \frac{d\epsilon_v}{dt} \right|_{switch} = 0; \quad (21)$$

$$\left. \frac{d^2\epsilon_v}{dt^2} \right|_{switch} < 0. \quad (22)$$

During the entire unloading path, the time shift factor is kept constant and is computed using the value of  $\epsilon_v$  at the switch point. The reverse switching from unloading to loading occurs when Eq. (21) is again satisfied and Eq. (22) is reversed.

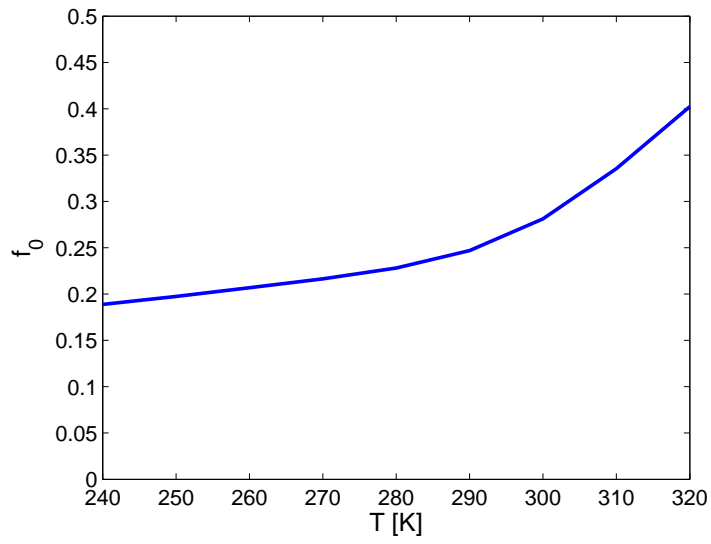


Figure 2: Reference fractional free volume.

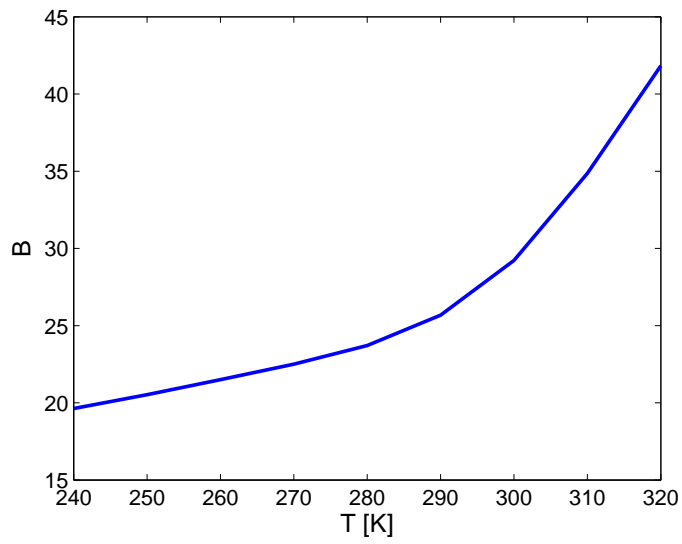


Figure 3: Material function  $B$  in the time shift factor of the free volume model.

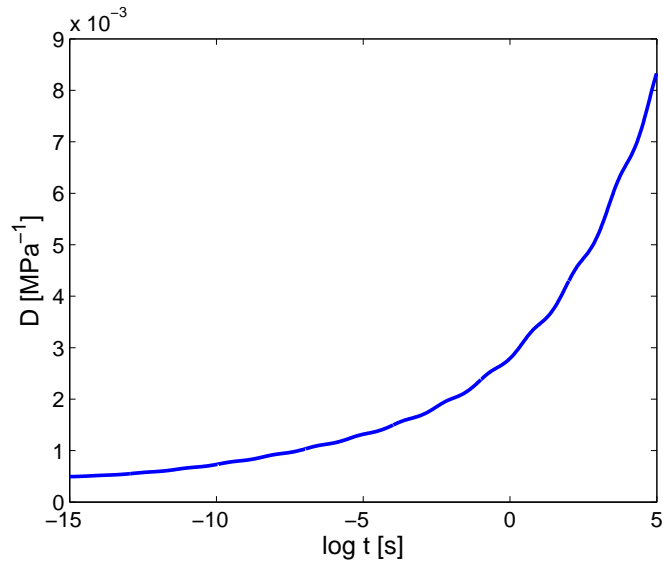


Figure 4: Master curve of the machine direction compliance at  $T_0 = 293.16$  K.

$j$	$D_{11,j}$ [ $MPa^{-1}$ ]	$\rho_j$ [s]
0	$3.0000 \times 10^{-4}$	—
1	$1.8764 \times 10^{-4}$	$1.6548 \times 10^{-16}$
2	$2.9249 \times 10^{-5}$	$4.8697 \times 10^{-15}$
3	$5.8224 \times 10^{-5}$	$1.4330 \times 10^{-13}$
4	$8.7542 \times 10^{-5}$	$4.2170 \times 10^{-12}$
5	$1.1561 \times 10^{-4}$	$1.2409 \times 10^{-10}$
6	$1.4159 \times 10^{-4}$	$3.6517 \times 10^{-9}$
7	$1.6989 \times 10^{-4}$	$1.0746 \times 10^{-7}$
8	$2.0924 \times 10^{-4}$	$3.1623 \times 10^{-6}$
9	$2.7274 \times 10^{-4}$	$9.3057 \times 10^{-5}$
10	$3.7796 \times 10^{-4}$	$2.7264 \times 10^{-3}$
11	$5.4670 \times 10^{-4}$	$8.0584 \times 10^{-2}$
12	$8.0581 \times 10^{-4}$	2.3714
13	$1.1844 \times 10^{-3}$	69.783
14	$1.7204 \times 10^{-3}$	2053.5
15	$2.6285 \times 10^{-3}$	60430

Table 1: Prony series representation of  $D_{11}$ .

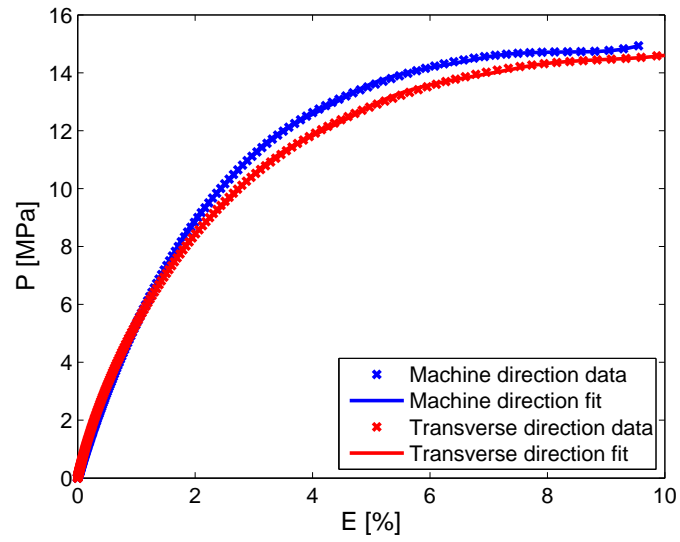


Figure 5: Uniaxial calibration tests on two different specimens, at a temperature of  $0^\circ$  and a strain rate of  $0.1\%/s$ .

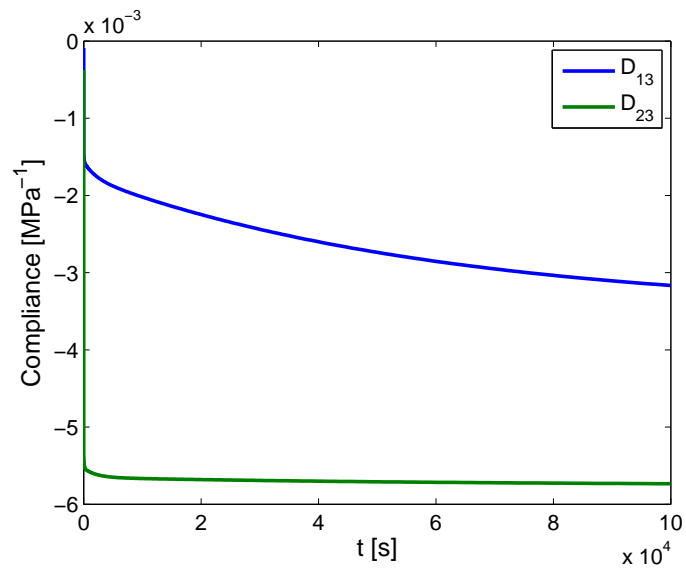


Figure 6: Master curves of  $D_{13}$  and  $D_{23}$ .



$j$	$D_{13,j} [MPa^{-1}]$	$D_{23,j} [MPa^{-1}]$
0	$-8.8901 \times 10^{-5}$	$-3.7419 \times 10^{-4}$
1	$-5.6735 \times 10^{-5}$	$-5.7000 \times 10^{-5}$
2	$-3.3813 \times 10^{-5}$	$-1.3669 \times 10^{-4}$
3	$-9.2295 \times 10^{-5}$	$-1.9696 \times 10^{-5}$
4	$-5.0846 \times 10^{-6}$	$-9.7338 \times 10^{-6}$
5	$-5.6338 \times 10^{-5}$	$-7.5581 \times 10^{-4}$
6	$-1.4242 \times 10^{-4}$	$-3.4473 \times 10^{-4}$
7	$-5.7724 \times 10^{-5}$	$-5.0554 \times 10^{-4}$
8	$-1.3820 \times 10^{-4}$	$-1.7405 \times 10^{-4}$
9	$-1.9962 \times 10^{-4}$	$-6.0937 \times 10^{-4}$
10	$-3.1119 \times 10^{-4}$	$-1.6420 \times 10^{-3}$
11	$-1.3591 \times 10^{-4}$	$-4.4417 \times 10^{-4}$
12	$-1.0536 \times 10^{-4}$	$-2.4046 \times 10^{-4}$
13	$-1.3895 \times 10^{-4}$	$-2.1729 \times 10^{-4}$
14	$-1.9557 \times 10^{-4}$	$-1.2279 \times 10^{-4}$
15	$-1.7442 \times 10^{-3}$	$-1.0191 \times 10^{-4}$

Table 2: Prony coefficients for  $D_{13}$  and  $D_{23}$ .

## IV. Finite Element Implementation

The anisotropic plane stress model developed in Sec. III was implemented in the commercial finite element code Abaqus/Standard through a user-defined material (UMAT) subroutine. A recursive numerical algorithm is utilized for computing the convolution integral in Eq. (11). We first describe the Abaqus interface and the overall computational scheme in the UMAT subroutine, then derive the discretized forms of the constitutive equations based on the recursive algorithm.

### A. General Scheme

At each iteration in the overall solution process, the Abaqus solver passes to the UMAT subroutine the time increment size  $\Delta t$  and the corresponding deformation gradients at the end of the current increment  $[F_t]$ . The role of UMAT is to update the Cauchy stress  $[\sigma_t]$  and the tangent stiffness.

The UMAT subroutine first uses the volumetric strain at the end of the previous time increment  $\epsilon_{v,t-\Delta t}$  to decide whether a switch from loading to unloading is required, and computes the time shift factor  $a_{t-\Delta t}$  using the chosen volumetric strain and the given temperature  $T$ . The current in-plane second Piola-Kirchhoff stresses  $[P_t]$  are obtained from the constitutive equations based on  $a_{t-\Delta t}$  and  $[F_t]$ , and finally pushed forward to the Cauchy stresses  $[\sigma_t]$  for returning to the Abaqus solver. The through-thickness strain  $E_{33,t}$  and the volumetric strain  $\epsilon_{v,t}$  are now determined from the known  $[P_t]$  and stored together with other history state variables for the next iteration.

It is noted that the stress update is based on  $a_{t-\Delta t}$ , instead of relying on an iterative scheme to arrive at a closer approximation for the current increment. Such an explicit integration approach is augmented by a step size adjustment process to maintain the accuracy of the solution. In this procedure, the time increment is reduced until a specified tolerance on the change in volumetric strain  $\Delta\epsilon_v$  is satisfied. The stresses are computed using the smallest time step. The complete flow of these numerical steps is depicted in Fig. (7).

### B. Loading/Unloading Switch Rule

Numerically, the criterion for switching described by Eqs. (21) and (22) is realized by comparing the values of volumetric strain at consecutive time steps. The time shift factor is determined according to

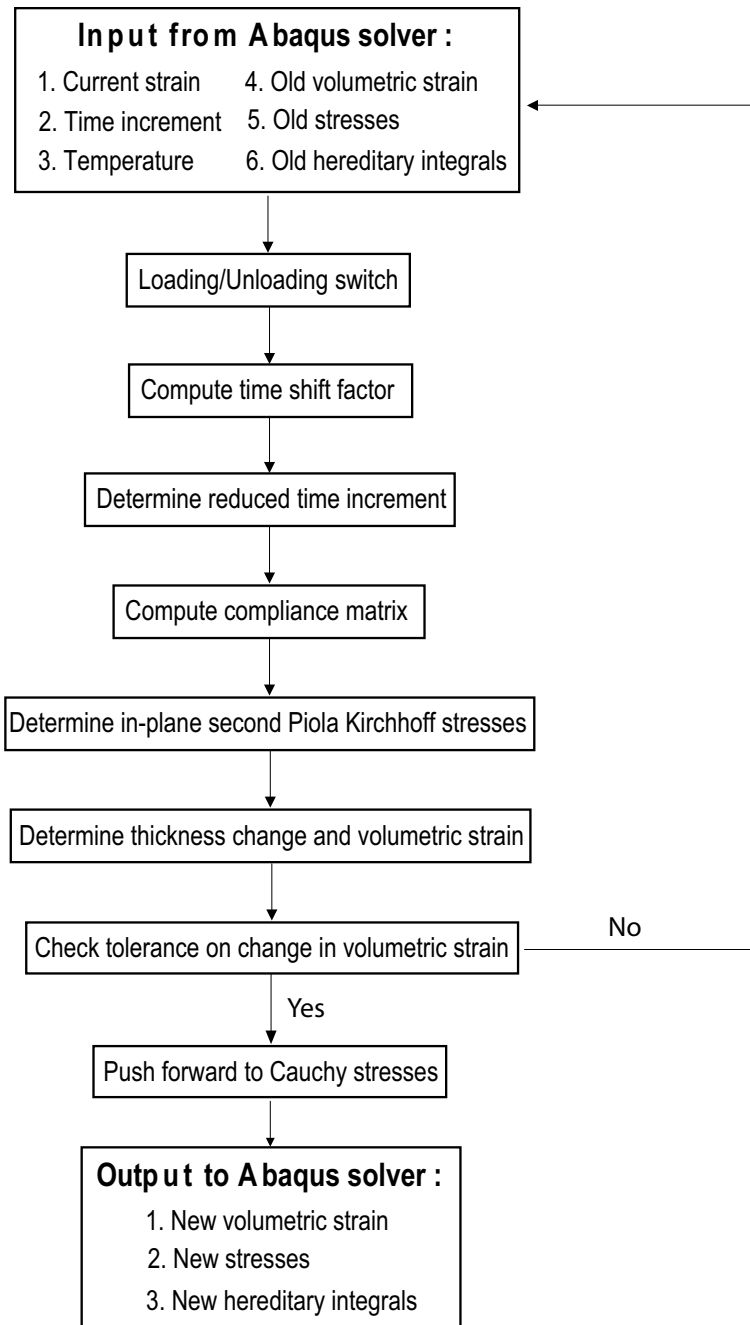


Figure 7: Free volume viscoelastic algorithm implemented in Abaqus UMAT.

$$\begin{aligned} a_{t-\Delta t} &= a(T_{t-\Delta t}, \epsilon_{v,t-\Delta t}) & \text{if } \epsilon_{v,t-\Delta t} \geq \epsilon_{v,t-2\Delta t}; \\ a_{t-\Delta t} &= a(T_{t-\Delta t}, \epsilon_{v,s}) & \text{if } \epsilon_{v,t-\Delta t} < \epsilon_{v,t-2\Delta t}. \end{aligned} \quad (23)$$

where  $s$  is the time at which loading switches to unloading. For an element loaded from its unstressed configuration at  $t = 0$ , the first instance  $\epsilon_{v,t-\Delta t} < \epsilon_{v,t-2\Delta t}$  is detected identifies the first switching point. It follows that a local maximum volumetric strain is located at  $t - 2\Delta t$  and therefore  $\epsilon_{v,s} = \epsilon_{v,t-2\Delta t}$ . This value of the volumetric strain is stored and used for computing  $a_{t-\Delta t}$  until when  $\epsilon_{v,t-\Delta t} \geq \epsilon_{v,t-2\Delta t}$  is detected again. The model uses the closest local maximum volumetric strain to compute the time shift factor during unloading for each cycle.

### C. Recursive Integration Algorithm

Taylor et al.<sup>22</sup> first proposed a recursive algorithm for linear viscoelastic integrals. With this algorithm, only the history variables at the previous time step are required for determining the current stress state. This approach minimizes the storage required to perform the integration. Similar algorithms have been implemented by Henriksen,<sup>23</sup> Lai and Bakker,<sup>24</sup> and Haj-Ali and Muliana<sup>25</sup> for the Schapery nonlinear viscoelastic integrals. In the current work the approach by Lai and Bakker was modified for the free volume model. For brevity, we present here only the recursive numerical algorithm for the case of uniaxial deformation.

We begin by substituting the creep compliance Prony series, Eq. (1), into the integral expression for the current strain, Eq. (4), to obtain

$$E_t = D_0 P_t + \sum_{j=1}^n D_j P_t - \sum_{j=1}^n D_j q_{j,t}, \quad (24)$$

where

$$q_{j,t} = \int_0^t e^{-(t'-\tau')/\rho_j} \dot{P}(\tau) d\tau. \quad (25)$$

The hereditary integral  $q_{j,t}$  can be rewritten in a recurrence relation with  $q_{j,t-\Delta t}$  assuming  $P$  varies linearly over the increment  $\Delta t$ :

$$q_{j,t} = e^{-\Delta t'/\rho_j} q_{j,t-\Delta t} + (P_t - P_{t-\Delta t}) \frac{1 - e^{-\Delta t'/\rho_j}}{\Delta t'/\rho_j}, \quad (26)$$

where  $\Delta t'$  is the reduced time increment computed assuming the time shift factor is constant over  $\Delta t$ :

$$\Delta t' = \frac{\Delta t}{a_{t-\Delta t}}, \quad (27)$$

$$\log a_{t-\Delta t} = \frac{-B_{t-\Delta t}}{2.303 f_{0,t-\Delta t}} \left[ \frac{\alpha_{v,t-\Delta t}(T_{t-\Delta t} - T_0) + \epsilon_{v,t-\Delta t}}{f_{0,t-\Delta t} + \alpha_{v,t-\Delta t}(T_{t-\Delta t} - T_0) + \epsilon_{v,t-\Delta t}} \right]. \quad (28)$$

The current total strain is obtained by substituting Eq. (26) into Eq. (24) and rearranging:

$$E_t = \left[ D_0 + \sum_{j=1}^n D_j - \sum_{j=1}^n D_j \frac{1 - e^{-\Delta t'/\rho_j}}{\Delta t'/\rho_j} \right] P_t - \sum_{j=1}^n D_j \left[ e^{-\Delta t'/\rho_j} q_{j,t-\Delta t} - \frac{1 - e^{-\Delta t'/\rho_j}}{\Delta t'/\rho_j} P_{t-\Delta t} \right]. \quad (29)$$

The second term in Eq. (29) is dependent only on information at  $t - \Delta t$  which is already known at the current increment. The current stress  $P_t$  is inverted from this expression with the suggested  $E_t$  by the Abaqus solver. The volumetric strain  $\epsilon_{v,t}$  is determined from

$$\epsilon_{v,t} = J_t - 1. \quad (30)$$

Finally the hereditary integrals  $q_{j,t}$ , second Piola-Kirchhoff stresses  $P_t$  and volumetric strain  $\epsilon_{v,t}$  are stored for use in the next increment.

## V. Verification of Model Predictions

The accuracy of the nonlinear viscoelastic model with the switching rule implemented in Abaqus is assessed by comparison to experimental data obtained from cyclic tests under controlled conditions. Test cases with uniform stress distribution are chosen and described in this section.

### A. Experiments

Biaxial tension and in-plane shear experiments were conducted on cylindrical specimens with a diameter of 100 mm and height of 270 mm. The specimens were fabricated by bonding with a heat sealer two 38  $\mu\text{m}$  thick rectangular pieces of StratoFilm 420. This construction technique provided two diametrically opposite seams that balance the stiffness distribution and thus avoid that the cylinder bends when it is loaded axially. Each end of the cylinders was bonded and clamped around the rim of a wooden disc acting as an end-fitting for connection with the load frame. The bottom fitting was equipped with two air ports for inflation and pressure measurements. Reflective targets were adhered to the cylinder surface for strain measurements using laser extensometers. A type-T thermocouple and a differential pressure transducer were used to monitor the temperature and pressure throughout the tests. The test setup is shown in Fig. (8).

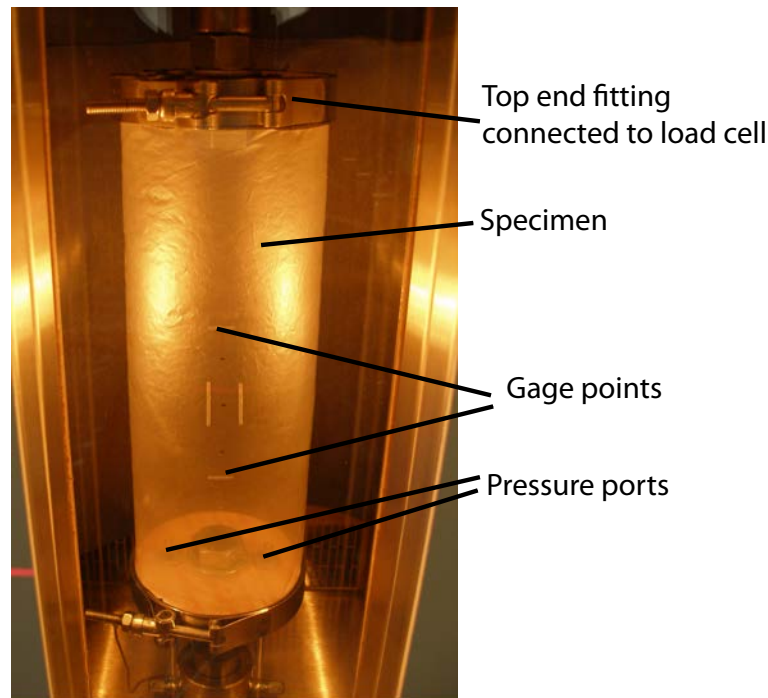


Figure 8: Cylindrical specimen mounted inside a thermal chamber.

For the biaxial tension tests, the cylinders were first inflated to the required pressure over a period of 10 s to provide hoop stress. Once the set pressure had been reached, the specimens were stressed axially by the load frame at a rate of 0.1 MPa/s for one cycle. For investigation of shear behavior, the cylinder was oriented such that the loading direction was at  $45^\circ$  from either material direction. This creates a shear stress in the material frame of reference. The pressure, axial load, temperature, axial and transverse strains were measured synchronously over time. The test conditions are summarized in Table 3.

### B. Finite Element Analysis

A finite element model of the cylinder was constructed in Abaqus/Standard to test the validity of the model and the numerical algorithm by comparing simulations with the tests conducted. The mesh consisted of 208 M3D4 square membrane elements, which were given the material properties described in Sec. III and IV. The interface between Abaqus and UMAT was established through \*USER MATERIAL. A material coordinate

Test	Type of test	Axial loading direction	Pressure [Pa]	Temperature [C]
1	Biaxial tension	Machine direction	700	-10
2	Biaxial tension	Transverse direction	400	0
3	In-plane shear	45° from machine direction	150	0

Table 3: Validation test parameters.

system was defined on all elements such that the material directions varied according to the load case being considered in Table 3.

Boundary conditions were imposed on the two ends of the cylinder. One end was fully constrained while the other was constrained in the radial direction, but free to translate in the axial direction. Geometrically nonlinear analyses were carried out. A uniform pressure was applied on all elements through the command \*DLOAD and the axial load was imposed on the nodes at the partially constrained end using \*CLOAD. The test conditions in Table 3 were replicated in the simulations.

### C. Comparison of Results

The stress-strain behavior for the biaxial tension and shear tests is plotted in Figs. (9)-(11), where it can be seen that the general features of each response have been satisfactorily reproduced. With the switch rule, the viscoelastic model treats loading and unloading differently. This allows the correct unloading path curvature to be predicted. It is worthwhile to mention that strain continues to increase with decreasing load for a short period of time before it reduces with load during unloading. This is a typical result of viscoelastic material under load control mode. The increase in strain in the initial part of the unloading segment is due to the prior loading, whose effect diminishes with time until the effect of unloading on the material eventually dominates. Close agreement is achieved between simulations and experimental data for the loading path for all three load cases presented. Despite having the correct curvature, the model predictions for the unloading path show some discrepancy with the measured response. In particular the model underestimates the strain and the errors in strain grow in size as the load decreases. In the fully unloaded state, the discrepancies are about 1.5%, 1% and 2% for tests 1, 2 and 3 respectively. Good correlation is obtained also in the plots of strain response over time for both material directions (tests 1 and 2) as illustrated in Figs. (12) and (13), except for the same kind of discrepancy described earlier for the unloading path.

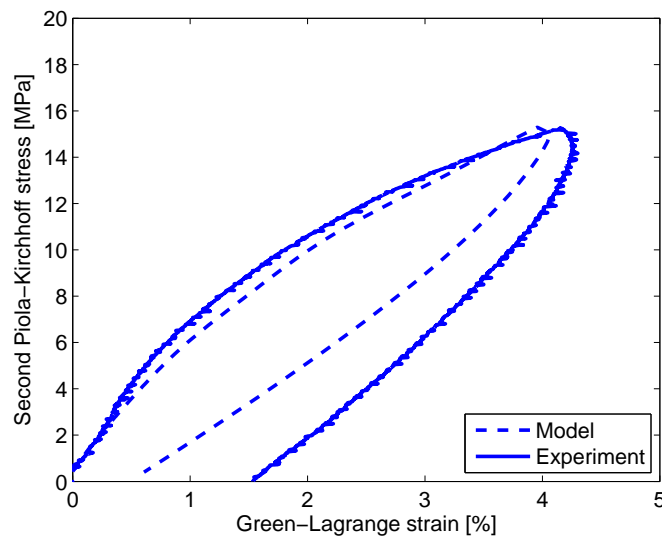


Figure 9: Stress vs. strain plots for test 1.

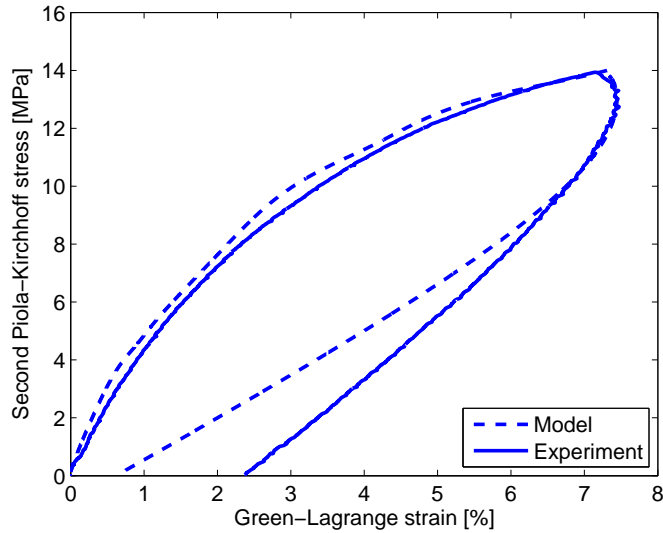


Figure 10: Stress vs. strain plots for test 2.

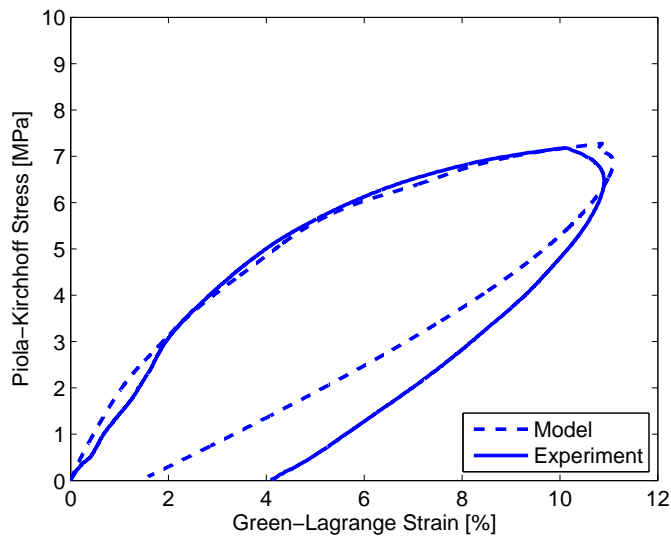


Figure 11: Stress vs. strain plots for test 3.

## VI. Discussion and Conclusion

An anisotropic viscoelastic constitutive model for large strain behavior has been formulated for the film material currently used for NASA superpressure balloon. The kinematics of the model are described with finite deformation measures and nonlinear material behavior is characterized by a time shift factor that is dependent on the volumetric strain. A switching rule that distinguishes between loading and unloading behavior is incorporated into the model and found capable of predicting the correct curvature of the unloading path, a feature that had not been previously captured by nonlinear viscoelastic models. A numerical algorithm for the proposed model has been developed and implemented in the finite element analysis program Abaqus/Standard via a user-defined material subroutine that utilizes an explicit and recursive numerical

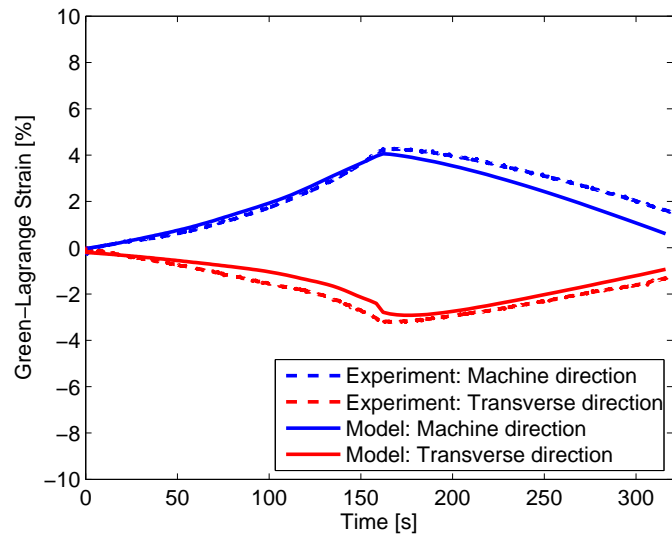


Figure 12: Strain vs. time plots for test 1.

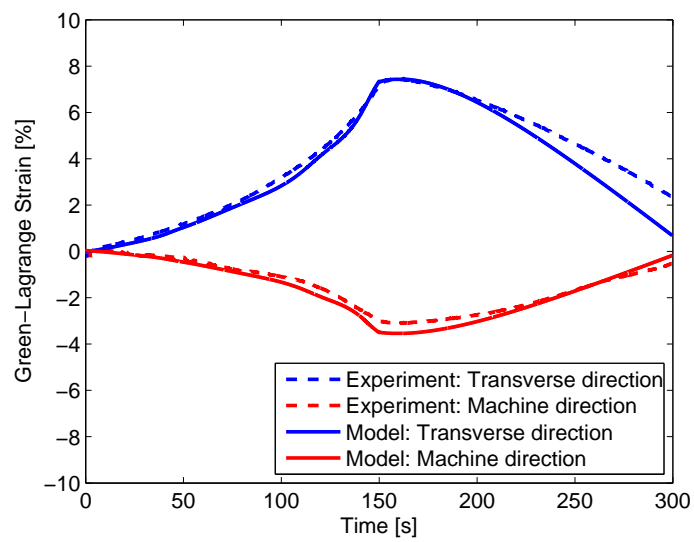


Figure 13: Strain vs. time plots for test 2.

time integration method. Model predictions of cyclic biaxial tension and shear stress states have been compared with experiments conducted on inflated cylindrical specimens under controlled thermal conditions. The results show good agreement between experiments and numerical simulations, except that the model consistently overestimates the strain recovery during unloading; this discrepancy increases as the specimen gradually approaches the zero stress configuration. Since the model had been “calibrated” against the loading parts only of two tension tests, it is not surprising that the unloading predictions are less accurate. It is concluded that the viscoelastic model and the numerical algorithm have been verified as able to capture the large strain behavior of balloon film with reasonable accuracy.

While only uniform stress states are investigated in detail in the present paper, wrinkling is expected to occur in regions of stress concentrations in thin membranes. An orthotropic wrinkling model is currently being assimilated into the viscoelastic material model.

## Acknowledgements

We thank Dr. Wolfgang Knauss (California Institute of Technology) and Dr. James Rand (Winzen Engineering Inc.) for helpful comments and discussions. Financial support from the Croucher Foundation (Hong Kong) and the NASA Balloon Program Office is gratefully acknowledged.

## References

- <sup>1</sup>Smith, I., “The NASA balloon program: Looking to the future,” *Advances in Space Research*, Vol. 33, 2004, pp. 1588–1593.
- <sup>2</sup>Smith, M. and Rainwater, E., “Optimum designs for superpressure balloons,” *Advances in Space Research*, Vol. 33, 2004, pp. 1688–1693.
- <sup>3</sup>Rand, J. and Sterling, W., “A constitutive equation for stratospheric balloon materials,” *Advances in Space Research*, Vol. 37, 2006, pp. 2087–2091.
- <sup>4</sup>Schapery, R., “An engineering theory of nonlinear viscoelasticity with applications,” *International Journal of Solids and Structures*, Vol. 2, 1966, pp. 407–425.
- <sup>5</sup>Schapery, R., “On the characterization of nonlinear viscoelastic materials,” *Polymer Engineering and Science*, Vol. 9, 1969, pp. 295–310.
- <sup>6</sup>Schapery, R., “Nonlinear viscoelastic and viscoplastic constitutive equations based on thermodynamics,” *Mechanics of Time-Dependent Materials*, Vol. 1, 1997, pp. 209–240.
- <sup>7</sup>Gerngross, T. and Pellegrino, S., “Anisotropic viscoelasticity and wrinkling of superpressure balloons: simulation and experimental verification,” *AIAA Balloon Systems Conference*, Seattle, WA, 2009.
- <sup>8</sup>Rand, J. and Wakefield, D., “Studies of thin film nonlinear viscoelasticity for superpressure balloons,” *Advances in Space Research*, Vol. 45, 2010, pp. 56–60.
- <sup>9</sup>Knauss, W. and Emri, I., “Nonlinear viscoelasticity based on free volume consideration,” *Computers and Structures*, Vol. 13, 1981, pp. 123–128.
- <sup>10</sup>Knauss, W. and Emri, I., “Volume change and the nonlinearly thermo-viscoelastic constitution of polymers,” *Polymer Engineering and Science*, Vol. 27, 1987, pp. 86–100.
- <sup>11</sup>O’Dowd, N. and Knauss, W., “Time dependent large principal deformation of polymers,” *Journal of Mechanics and Physics of Solids*, Vol. 43, 1995, pp. 771–792.
- <sup>12</sup>Popelar, C. and Liechti, K., “Multiaxial nonlinear viscoelastic characterization and modeling of a structural adhesive,” *Journal of Materials and Technology*, Vol. 119, 1997, pp. 205–210.
- <sup>13</sup>Popelar, C. and Liechti, K., “A distortion-modified free volume theory for nonlinear viscoelastic behavior,” *Mechanics of Time-Dependent Materials*, Vol. 7, 2003, pp. 89–141.
- <sup>14</sup>Xia, Z., Shen, X., and Ellyin, F., “An assessment of nonlinearly viscoelastic constitutive models for cyclic loading: The effect of a general loading/unloading rule,” *Mechanics of Time-Dependent Materials*, Vol. 9, 2006, pp. 281–300.
- <sup>15</sup>Zhang, C. and Moore, I., “Nonlinear mechanical response of high density polyethylene. Part II: Uniaxial constitutive modeling,” *Polymer Engineering and Science*, Vol. 37, 1997, pp. 414–420.
- <sup>16</sup>Arzoumanidis, G. and Liechti, K., “Linear viscoelastic property measurement and its significance for some nonlinear viscoelasticity models,” *Mechanics of Time-Dependent Materials*, Vol. 7, 2003, pp. 209–250.
- <sup>17</sup>Ferry, J., *Viscoelastic Properties of Polymers*, John Wiley and Sons, New York, 3rd ed., 1980.
- <sup>18</sup>Holzappel, G., *Nonlinear Solid Mechanics*, John Wiley and Sons, Chichester, 2000.
- <sup>19</sup>Rand, J., “An improved constitutive equation for SF420 Part I: the master curve,” Report by Winzen Engineering Inc., July 2008.
- <sup>20</sup>Rand, J., “An improved constitutive equation for SF420 Part II: the biaxial behavior,” Report by Winzen Engineering Inc., July 2008.
- <sup>21</sup>Young, L., “GSFC CTE curve fitting data,” Report by Goddard Space Flight Center, May 2010.
- <sup>22</sup>Taylor, R., Pister, K., and Goudreau, G., “Thermomechanical analysis of viscoelastic solids,” *International Journal for Numerical Methods in Engineering*, Vol. 2, 1970, pp. 45–59.



<sup>23</sup>Henriksen, M., “Nonlinear viscoelastic stress analysis - a finite element approach,” *Computers and Structures*, Vol. 18, 1984, pp. 133–139.

<sup>24</sup>Lai, J. and Bakker, A., “3-D Schapery representation for nonlinear viscoelasticity and finite element implementation,” *Computational Mechanics*, Vol. 18, 1996, pp. 182–191.

<sup>25</sup>Haj-Ali, R. and Muliana, A., “Numerical finite element formulation of the Schapery nonlinear viscoelastic material model,” *International Journal for Numerical Methods in Engineering*, Vol. 59, 2004, pp. 25–45.